Chinese Journal of Geotechnical Engineering

Volume 43 Issue 10 Year 2021

Evaluation of the Critical Responses of Flexible Pavement Structure with Stabilized Sabkha Base and Geogrid Reinforcement

Gamil M. S. Abdullah*
Civil Engineering Department, College of Engineering, Najran University, Kingdom of Saudi Arabia

Keywords: Sulfur Emulsified Asphalt; Marginal Soils; Geogrid; Sabkha; Finite Element Modeling; Stabilized Pavement

DOI:
10.11779/CJGE202110.2

ABSTRACT: Marginal and problematic soils such as dune sand and sabkha cover wide areas in the eastern, southern, and western parts of the Kingdom of Saudi Arabia in addition to the coastal line of the Arabian Gulf. The most common problems of these problematic soils are high compressibility, low shear strength, large volume change (especially in sabkha), and low bearing capacity. Therefore, this research reported a series of finite elements modeled by the Plaxis 3D software to evaluate the critical responses of pavement structures constructed using these marginal soils. The pavement structure consisted of a standard asphalt concrete layer, a base layer of sabkha soil treated with Emulsified Sulfur Asphalt (ESA), and a sand subbase layer. These layers were resting on the natural sabkha subgrade. The model's input parameters for each layer were a combination of laboratory and literature data. The simulation was done for a pavement section without reinforcement and another reinforced with geogrid positioned at different places to study the best location reducing critical responses, i.e., fatigue, rutting strains, and damage ratio. The hardening soil model was selected to model the nonlinear behavior of an ESA–sabkha base, sand subbase layer, and sabkha subgrade while the linear elastic model was used for asphaltic concrete layer and geogrid material. The simulation outcomes displayed that positioning geogrid reinforcement at the interface of an ESA–sabkha base and sand subbase layers led to the maximum decrease in horizontal tensile (fatigue strains) and vertical compressive strains (rutting strains) and vertical displacement. Furthermore, geogrid reinforcement decreased the fatigue damage ratio significantly (31 to 51%), while the reduction in rutting damage ratio was a little bit lower (11 to 25%). Finally, placing geogrid on the subgrade leads to a higher reduction in fatigue and rutting strains and vertical displacement.

1. INTRODUCTION

Marginal and problematic soils such as dune sand and sabkha cover wide areas in the eastern, southern, and western parts of the Kingdom of Saudi Arabia the Arabian Gulf shoreline. Akili (2006) reported that sabkha soil covers 20% of the Arabian Gulf coastal strip area, approximately 50,000 km^2, i.e., 1,000 km long with 50 km wide. Figure 1 shows sabkha soil distribution in the Kingdom of Saudi Arabia and the coastal line of the Arabian Gulf. The construction of roads in these areas without using the available local marginal soils, i.e., dune sand and sabkha, is not cost beneficial, not to mention the scarcity of good construction materials. Stabilization of the marginal and problematic soils including sabkha soil has proved its effectivity in enhancing their engineering properties, which can be done with any suitable stabilizers such as cement, cement kiln dust, emulsion asphalt, foamed asphalt, Emulsified Sulfur Asphalt (ESA), Foamed Sulfur Asphalt (FSA) Abdullah and Al-Abdul Wahhab, 2015, 2018; and *Al-Homidy et al. 2017*), lime, and many other familiar chemical stabilizers stated in literature.

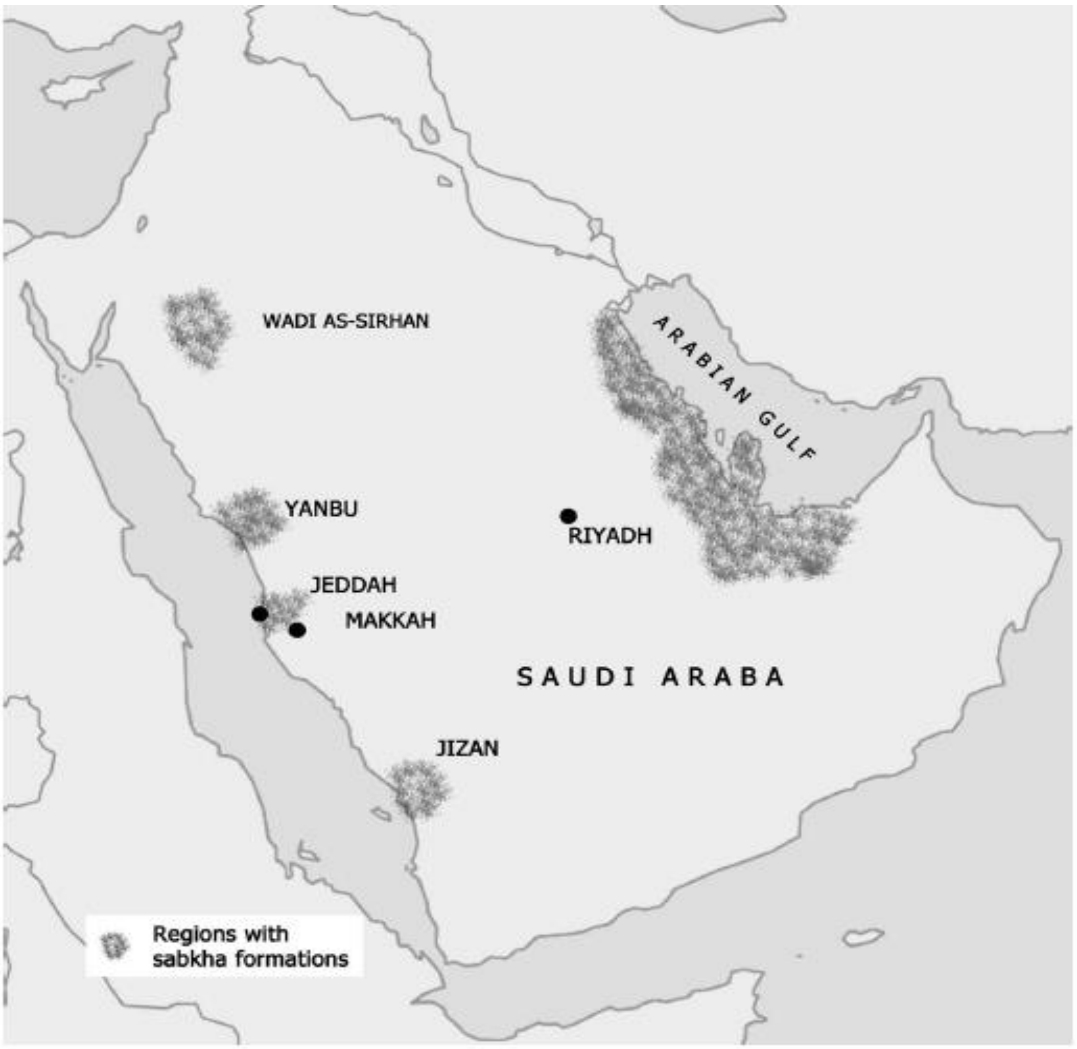

Figure 1. Sabkha soil distribution in the Kingdom of Saudi Arabia (after Abduljauwad and Al-Amoudi, 1995)

Over the few past decades, researchers have analyzed the performance of pavement structures with conventional materials using different simulation programs such as ANSYS, ABAQUS, Plaxis 2D, 3D, etc. The analysis was done for unreinforced and reinforced sections with geogrids, geotextiles, or any other reinforcement materials. Using geogrid strengthening in the building of pavement structures was introduced in the 1970s. Thereafter, the practice of geogrid reinforcement has been widely used and several laboratories and theoretical investigations were conducted to evaluate the behavior of flexible pavement structures reinforced with geogrid (Howard and Warren, 2009; Perkins, 2001, 2002; and *Berg et al. 2000*).

Finite elements were modeled via ABAQUS software used by *Wathugala et al. (1996)* to investigate the possibility of rut depth reduction due to the reinforcement of flexible pavement with the geogrid membrane at different locations. The geogrid was placed at the interface of base layer and subgrade, base, and asphalt concrete layers and inside the base layer at its first third of thickness from the bottom. The research showed the maximum reduction of the fatigue strains was attained, about 46 to 48% when geogrid was put between the asphaltic concrete and base layers.

Mousavi et al. (2017) evaluated the optimal position of the geogrid reinforcement inside the aggregate base layer in an unpaved road using the Plaxis 3D finite element modeling commercial software. Results showed that regardless of the thickness of the aggregate base course layer, the surface deformation was diminished when the geogrid membrane was placed at a distance equating to half of the radius of the loaded area (D = 0.5r).

Many Researchers and studies focused on this field using various 2D or 3D simulation programs and different constitutive models like the linear elastic, Mohr-coulomb, and hardening soil models. Some of them used plain strain and others used axisymmetric models according to the problem conditions (Ling and Liu, 2003; *Sukumaran et al. 2004*; *Pandey et al. 2012; Abdhesh et al. 2014*; Al-Azzawi, 2012 and Tapase and Ranadive, 2016). Some researchers recommended that the optimal place of geogrid reinforcement is at the interface of base and subbase layers while some others recommended using reinforcement between the subgrade and subbase course layers. All these outcomes imply that the location of geogrid reinforcement in a pavement structure is still an area of investigation and research.

Abdullah and Al-Abdul Wahhab, (2018) studied the potentiality of stabilizing sabkha soil, availing Emulsified Sulfur Asphalt (ESA), a new stabilizer in the field of soil stabilization called. ESA stabilizer is produced by replacing asphalt with 30% of sulfur. This stabilizer material, i.e., ESA, was a part of a patent investigated by the investigation group at the King Fahd University of Petroleum and Minerals (KFUPM) [Al-Mehthel, Al-Abdul Wahhab, Hussein and Al-Idi, 2017. Patent number is 11201604034Y (Docket Number: SA5095-06)]. The results of the study indicated that ESA–stabilized sabkha fulfilled the specifications in terms of indirect tensile strength, Marshal, and shear strength tests, where it can be used in the pavement structure such as base layers. However, the critical responses in terms of fatigue and rutting distress performance of this material (ESA sabkha) when used as a base layer in a pavement structure resting on sabkha subgrade were not studied.

In this research, finite element simulations were done using the commercial Plaxis 3D geotechnical-based software to simulate the performance and study the critical responses (fatigue, rutting strains, and damage ratio) of a pavement structure comprising of a standard asphaltic concrete layer, sabkha soil stabilized with Emulsified Sulfur Asphalt (ESA) base, and sand subbase layer used for drainage purposes. The layers of pavement structure are resting on the natural sabkha subgrade. The analysis was also performed on the previously mentioned pavement structure with additional geogrid reinforcement at various locations. The Plaxis 3D software was selected as the tool of analysis because it is a geotechnical-based software capable of perfectly representing and simulating soil–structure interactions besides easy modeling and self-adaptive mesh generation; Plaxis 3D analyses are always close and in agreement with the experimental work results. Thus, this study investigated the performance of a new stabilized base material (ESA sabkha) which performance has never been simulated or investigated yet.

2. FINITE ELEMENT MODELING

A typical section of flexible pavement comprising of a surface bituminous (HMA) layer, the base layer of stabilized sabkha, i.e., ESA sabkha, sand subbase layer, and a natural sabkha subgrade soil was modeled in a three-dimensional manner using the Plaxis 3D software shown in figure 2. The thicknesses of the surface bituminous, stabilized sabkha base, and subbase layers were 0.1, 0.15, and 0.3 m, respectively. The model was developed for pavement sections without reinforcement and with geogrid reinforcement at different locations as well. Axisymmetric modeling was selected and performed since it can simulate circular loading and does not require much time for computation. Due to the symmetry, only one quarter was modeled to reduce the computational time. Axisymmetric modeling was used by many investigators such as *Moayedi et al. (2009),* Kazemien et al. (2010), and Howard and Warren (2009) because of the advantages mentioned beforehand. For the appropriate boundaries of the model, Alex (2000) declared that the strains of nodal radial were generally anticipated to be ignored at around ten times the radius of the area of distributed loading representing utilized tire load. Furthermore, the nodular displacements and stresses were also expected to be not significant and ignored at twenty times the radius of the area of applied load under the pavement surface. Based on that, the length, width, and depth of the pavement section model were put as 3, 3, and 5 m, respectively (Howard and Warren, 2009). The finite element modeling was performed for pavement sections without geogrid and with geogrid placed at three locations. These locations are on the stabilized sabkha base layer, subbase layer, and, finally, subgrade layer.

Figures 3 shows the axisymmetric finite element modeling for a pavement section with geogrid placed at the interface of the asphaltic concrete and the ESA–sabkha base layers, whereas figure 4 shows the model when the geogrid positioned between the ESA–sabkha base and subbase layer.

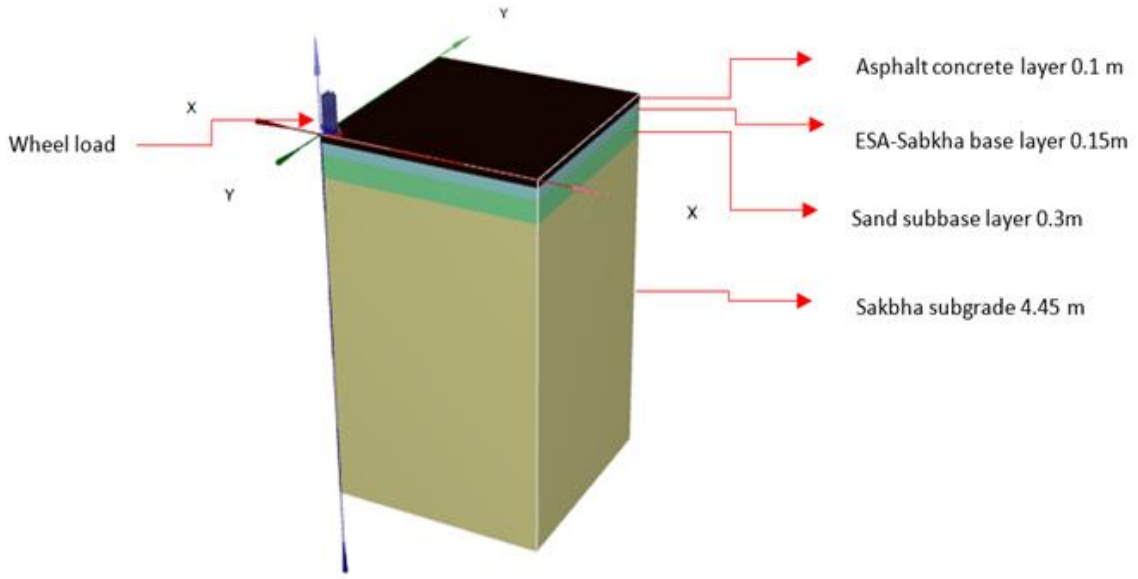

Figure 2. Geometry of axisymmetric finite element modeling of pavement section without geogrid

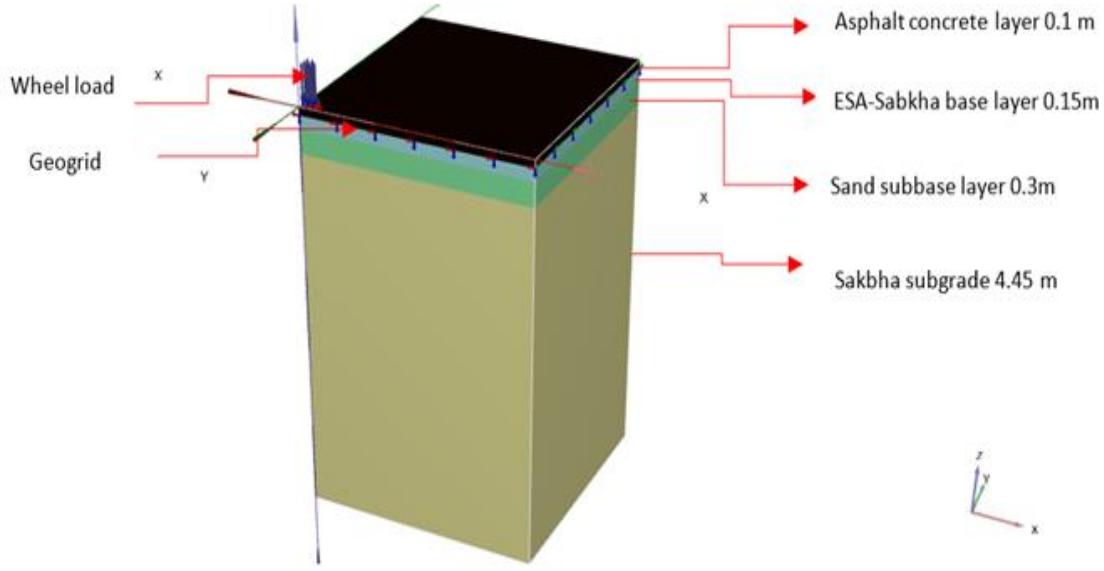

Figure 3. Axisymmetric finite element modeling of a geogrid-reinforced pavement structure at the top of stabilized ESA–sabkha base layer

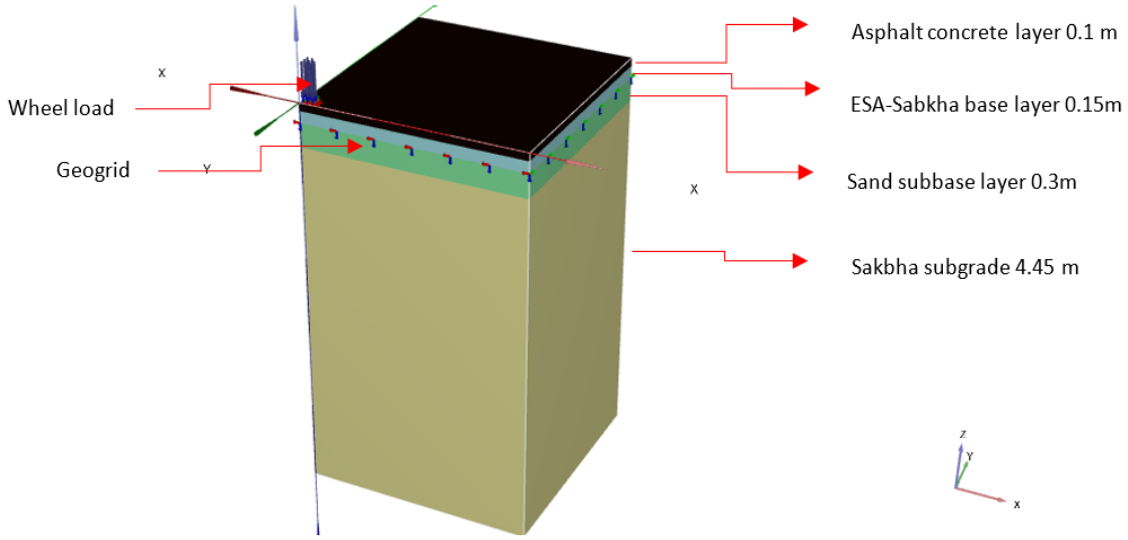

Figure 4. Axisymmetric finite element modeling of a geogrid-reinforced pavement structure at the bottom of stabilized ESA-sabkha base layer

2.1 Constitutive Models and Materials Parameters

The hardening soil model available in Plaxis 3D was used to model the nonlinear performance of the stabilized base, subbase, and subgrade materials. The hardening soil model is a hyperbolic stress strain model with limiting states resembling Mohr-Coulomb's by means of the friction angle ϕ, cohesion *c,* and the dilatancy angle ψ (*Schanz et al. 1999)*. In the hardening model, there are three different inputs of stiffness to represent the dependency of soil stiffness on applied stress. These inputs are the triaxial stiffness E50, the oedometer loading tangent stiffness E_{oed}, and the triaxial unloading stiffness Eur. In addition to secant, oedometric, and unloading–reloading stiffness, the model is defined by extra parameters such as reference stress and a power factor (p^{ref}, m). For the asphaltic concrete layer and reinforcement geogrid materials, a linear elastic isotropic model was selected to simulate their performance. The relation between the angle of dilation, ψ, and the angle of internal friction of the soil suggested by Bolton (1986) has been adopted.

The soil-geogrid element interface was simulated as rigid and there is no drop in interface strength, meaning that R_{inter} = 1.0, as recommended by Mirmoradi and Ehrlich (2015a) for geogrids. The physical meaning of presuming rigid interfaces is that the relative motion among the geogrid and soil interfaces is not allowed. The material properties and parameters utilized in the hardening finite element modeling are obtained from laboratory tests and literature data as given in table 1.

2.2 Loading, Boundary Conditions, and Meshing

Many factors affect the design of a flexible pavement system. These factors can be categorized into four groups: traffic and loading, structural models, material characterizations, and environmental conditions. Traffic is considered the greatest significant factor in designing a pavement structure. Tire pressure, wheel load, load movement and repetition, and configuration of axles are all key factors. Heavier vehicles are the main cause of distresses and failure of pavements. The contact area and pressure between the surface of the pavement and the wheel depend on the tire pressure. The real shape of the contact area is elliptical; however, scientists consider it as circular for purpose of analysis simplification. The radius of this circular area is defined based on tire contact pressure and wheel load. To model the dual wheel exercised load on the pavement surface, a contact pressure of about 550 kPa was utilized in the modeling as shown in figure 2. The tire contact pressure on the pavement is equivalent to tire inflation pressure with a circular area of a radius of 200 mm representing the tire imprint. The tire wall stiffening's effect was ignored. The boundary conditions adopted in the modeling are such that the model was constrained at the bottom and no movements in the directions vertical to the symmetry planes were considered, i.e., roller support.

Plaxis 3D can generate the mesh automatically as seen in figure 5. The mesh of the finite element model was established by utilizing ten-node tetrahedral elements to represent all pavement layers. The geogrid reinforcement was simulated using geogrid elements offered by the Plaxis 3D software, consisting of six-node triangular surface elements. The mesh size effect was avoided by using fine mesh analysis for reinforced and unreinforced pavement sections to get accurate results. The mesh generation created around 54,481 elements and 78,817 nodes in the unreinforced section and 86,619 elements and 122,752 nodes in the reinforced section.

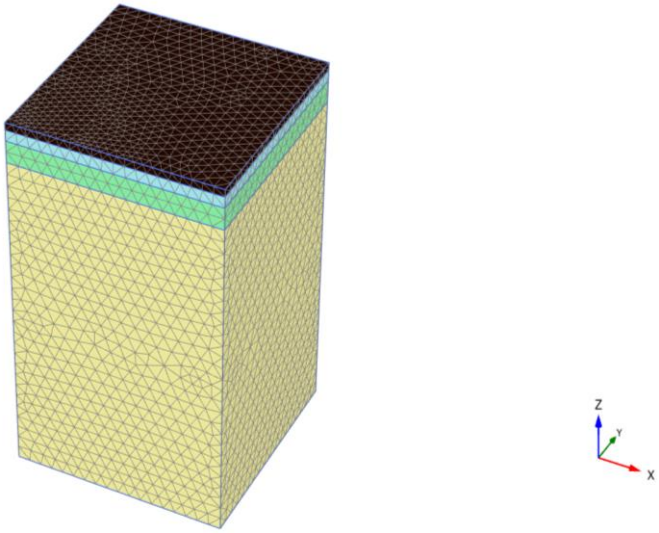

Figure 5. Finite element meshing

Table 1. Material parameters for the finite element modeling

Parameter	Asphaltic Concrete	Stabilized Base (ESA Sabkha)	Subbase (Sand)	Subgrade (Sabkha)	Geogrid
Thickness (mm)	100	150	300	4450	
Unsaturated Unit Weight, γ_{unsat} (KN/m^3)	20	19	17	15.5	
Saturated Unit Weight, γ_{sat} (KN/m^3)	-	20	18	17.5	
Material Model	Linear elastic	Hardening soil	Hardening soil	Hardening soil	
Drainage Type	non-porous	Drained	Drained	Drained	
E_{50} ref (KPa)		$8 * 10^5$	30000	6000	
E_{oed} ref (KPa)		$8 * 10^5$	30000	6000	
E_{ur} ref (KPa)		$2400 * 10^3$	90000	18000	
Power in Stiffness Laws, m		0.5	0.5	0.5	
Unloading–Reloading Poisson's Ratio v		0.2	0.2	0.2	
Cohesion, C (KN/m^2)		12	1	1	
Angle of Friction, φ (°)		30	35	34	
Angle of Dilatancy, Ψ (°)		0	5	4	
Interface Reduction Factor, R_{inter}	1	1	1	1	
Axial Stiffness, EA (KN/m)					960

3. RESULTS AND DISCUSSION

A parametric investigation was conducted to surmise the influence of the position of a geogrid membrane on the structural behavior of flexible pavement sections with a stabilized sabkha base layer. Three locations were selected to place the geogrid separately. First, the geogrid was positioned between the surface asphaltic concrete layer and stabilized sabkha base (ESA sabkha) layer. The second location was at the interface of the ESA–sabkha base and sand subbase layers. The last location was on the sabkha subgrade. Using the Plaxis 3D software, pavement critical responses such as fatigue and rutting strains (εt^{max} and εc^{max}) were calculated for all unreinforced and reinforced pavement sections. The tensile and compression strains (εt^{max} and εc^{max}) were estimated at bottom of the asphaltic concrete and stabilized base layers and the top of the subgrade, respectively. Table 2 presents the predicted responses of all cases.

Based on the presented results, it is seen that fatigue strains (horizontal strain) at the bottom of the asphaltic concrete layer were reduced by 2.1% when the pavement was reinforced with a geogrid located at the interface of bituminous concrete and a stabilized sabkha base layer. However, a decrease of approximately 21.1% in fatigue strains was achieved when the geogrid was placed at the bottom of the stabilized sabkha base layer while a decrease of 22.8% was achieved when placed on the subgrade. It is clear that when the geogrid reinforcement is placed at the bottom of the stabilized base layer, it substantially helps reduce the horizontal fatigue tensile strain developed at the interface. This could be attributed to the high modulus of the stabilized sabkha base layer—thus high layer stiffness, making it behave almost like the top asphaltic layer in fatigue resistance.

Table 2. Fatigue, rutting strains, and vertical displacement predicted through the finite element model

Geogrid Location	**εt^{max} ($x10^{-3}$)**	**εc^{max} ($x10^{-3}$)**	**Total Displacement $\|u\|$ ($x10^{-3}$) m**
Unreinforced Pavement	4.292	1.873	9.671
Geogrid at the top of ESA–Sabkha Base.	4.204	1.846	9.555
Geogrid at the Bottom of ESA–Sabkha Base (Top of Subbase)	3.387	1.770	9.348
Geogrid at the Top of Subgrade	3.312	1.766	9.314

On the other hand, no significant reduction in the rutting strains (vertical strains) was observed in all cases of pavement geogrid reinforcement. The maximum reduction was noticed when the geogrid was put on the sabkha subgrade and was about 5.7%. Similarly, marginal differences in total vertical displacement under the load were found between unreinforced pavement and geogrid-reinforced sections. Maximum reduction was at about 3.7% when the geogrid reinforcement was located on the subgrade. This could be attributed to the fact that geogrids are tensile-resistant materials and are not used mainly to reduce vertical displacement in most cases (*Pandey et.al. 2012; Majedi et al. 2017 and Ibrahim et al. 2017*). However, from table 2, it is noticed that the maximum reduction in fatigue and rutting strains and vertical displacement values are obtained when the geogrid is placed on the subgrade, concluding that this is the best location for the geogrid.

To reduce the number of figures, we only presented some samples of the Plaxis 3D analysis results for the unreinforced referenced pavement section and the case where the geogrid was positioned at the bottom of the ESA–sabkha base layer, as it was found to be the best location for enhancing the pavement section engineering properties. Thus, figures 6–8 show the horizontal and vertical strains and absolute vertical displacement for unreinforced pavement while figures 9–11 present the same parameters for pavement structure with geogrid reinforcement at the bottom of the ESA–sabkha base layer.

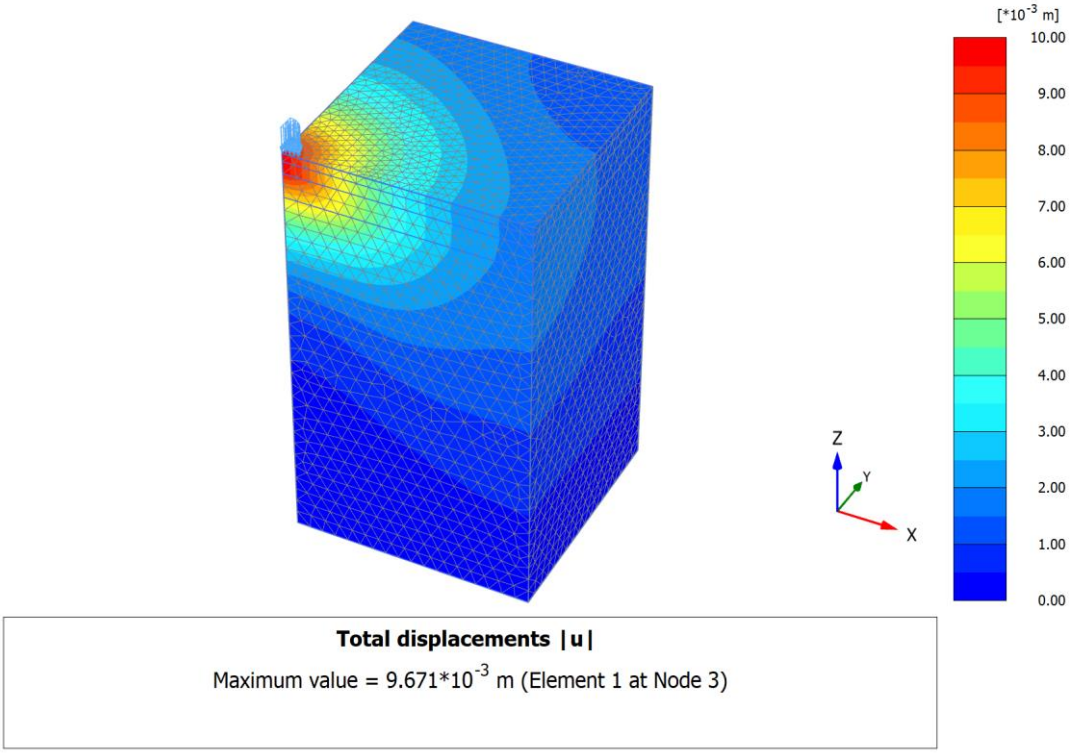

Figure 6. Total displacement for unreinforced pavement (applied tire pressure 550 kPa)

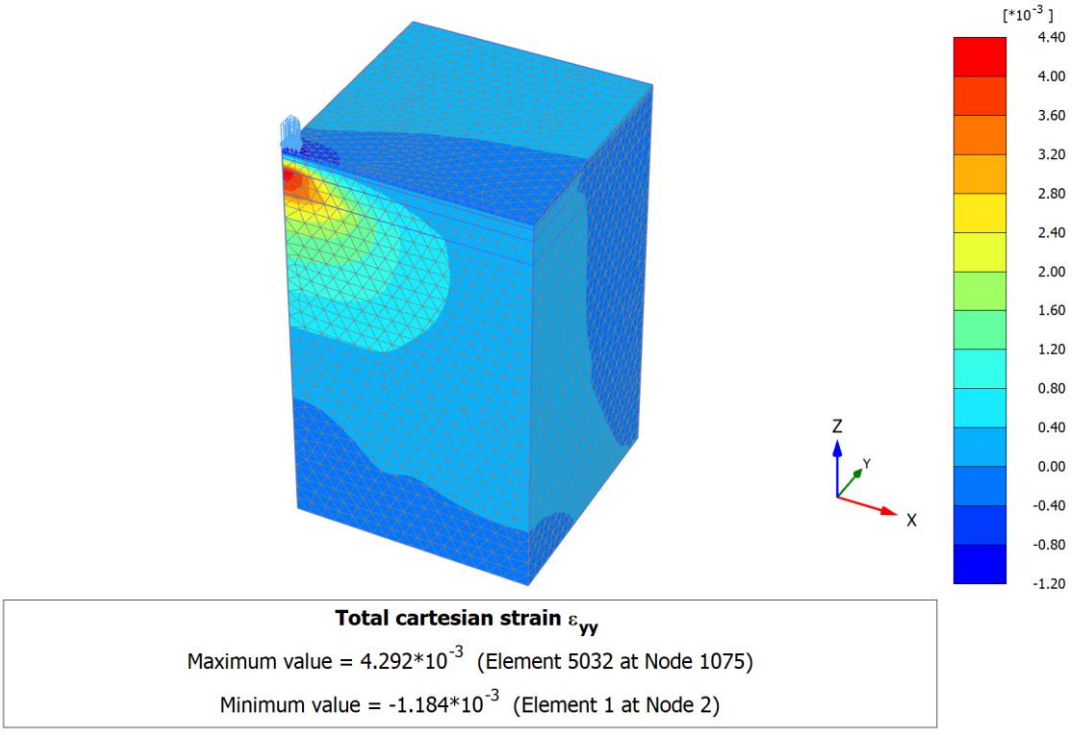

Figure 7. Horizontal strains for pavement without reinforcement (load 550 kPa)

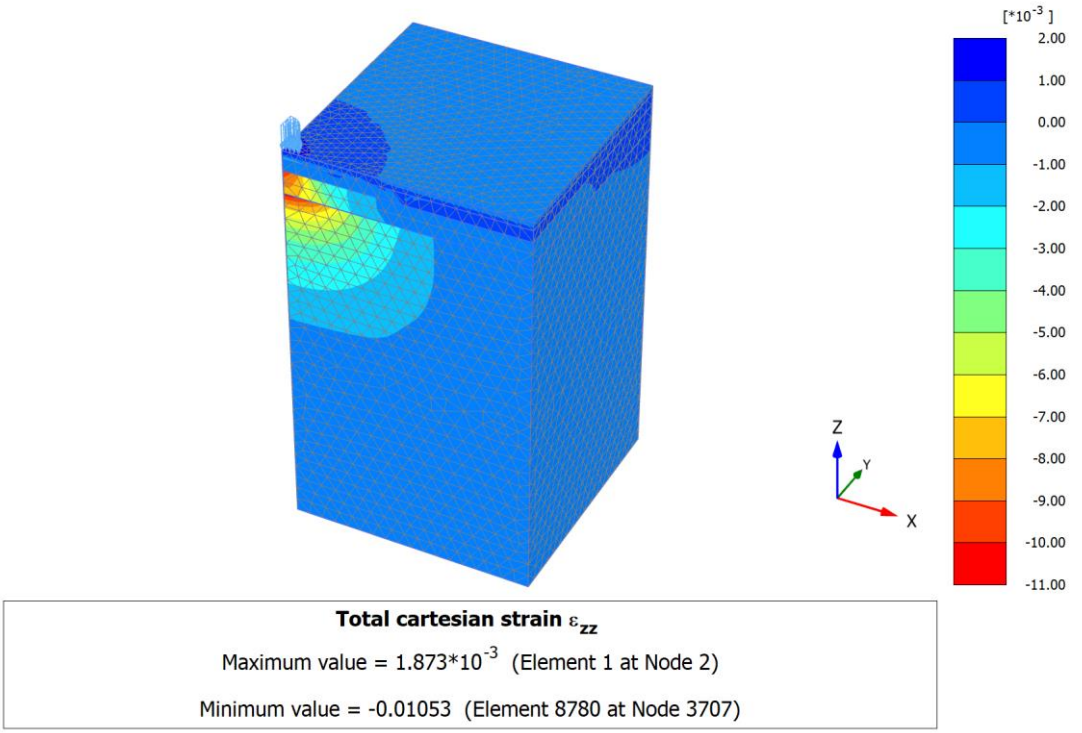

Figure 8. Vertical strains for pavement structure without reinforcement (load 550 kPa)

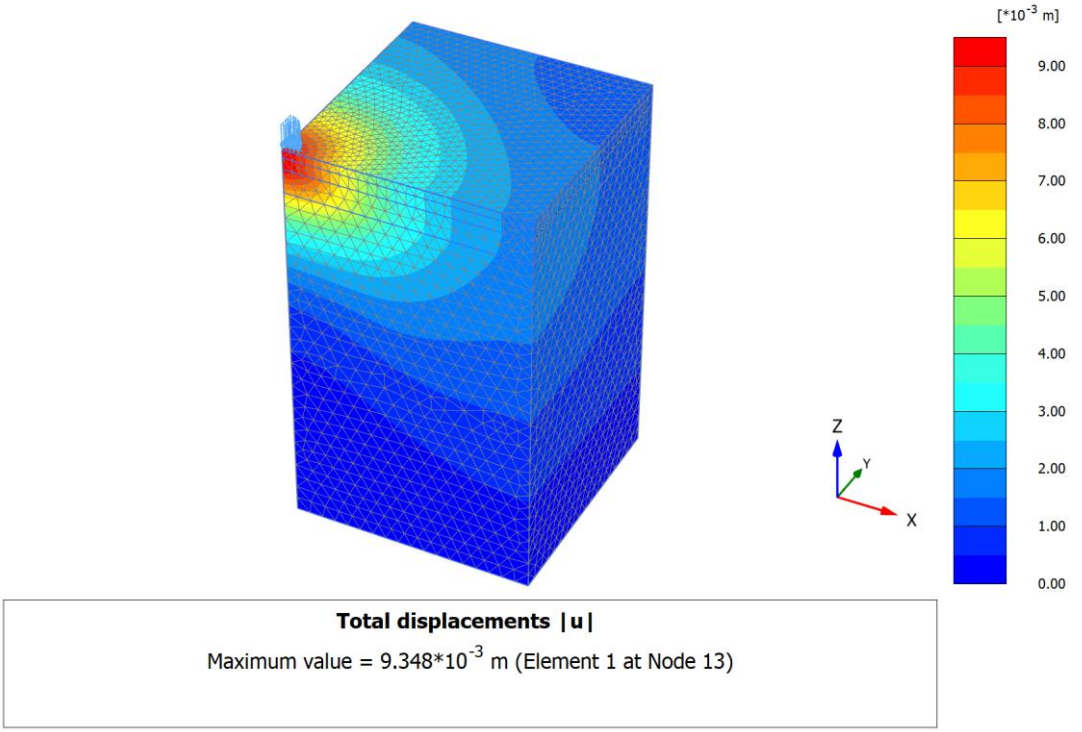

Figure 9. Total displacement for pavement structure with reinforcement at the bottom of the ESA–sabkha base layer (load 550 kPa)

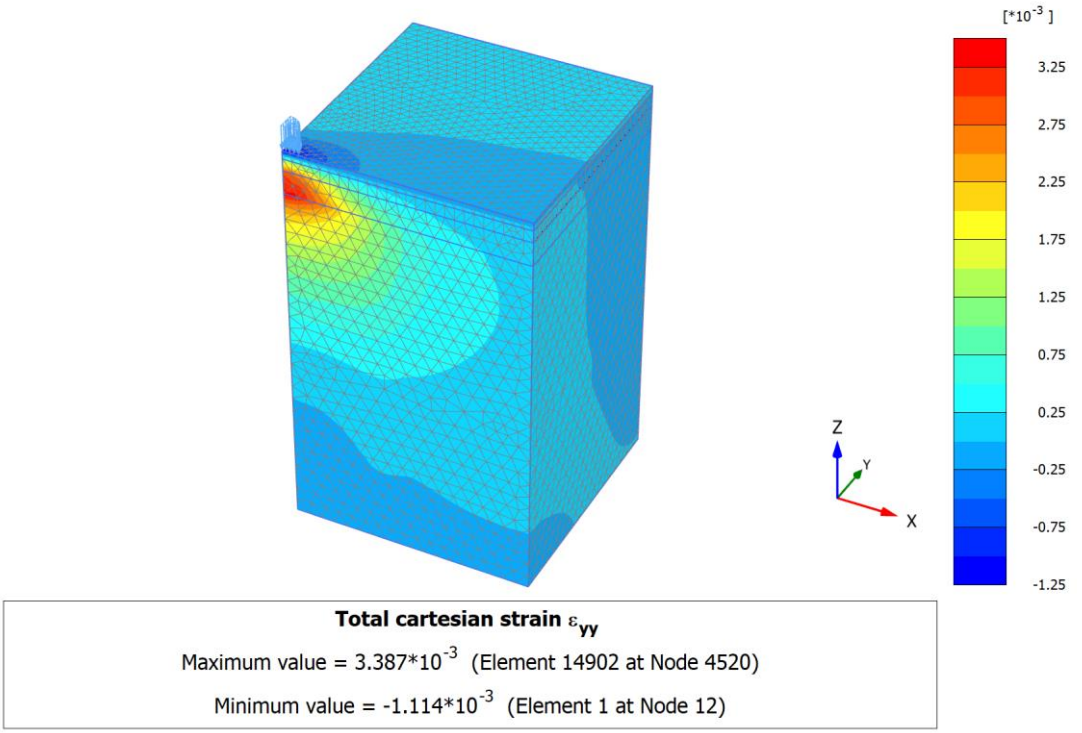

Figure 10. Horizontal strains for pavement structure with reinforcement at the bottom of the ESA–sabkha base layer (load 550 kPa)

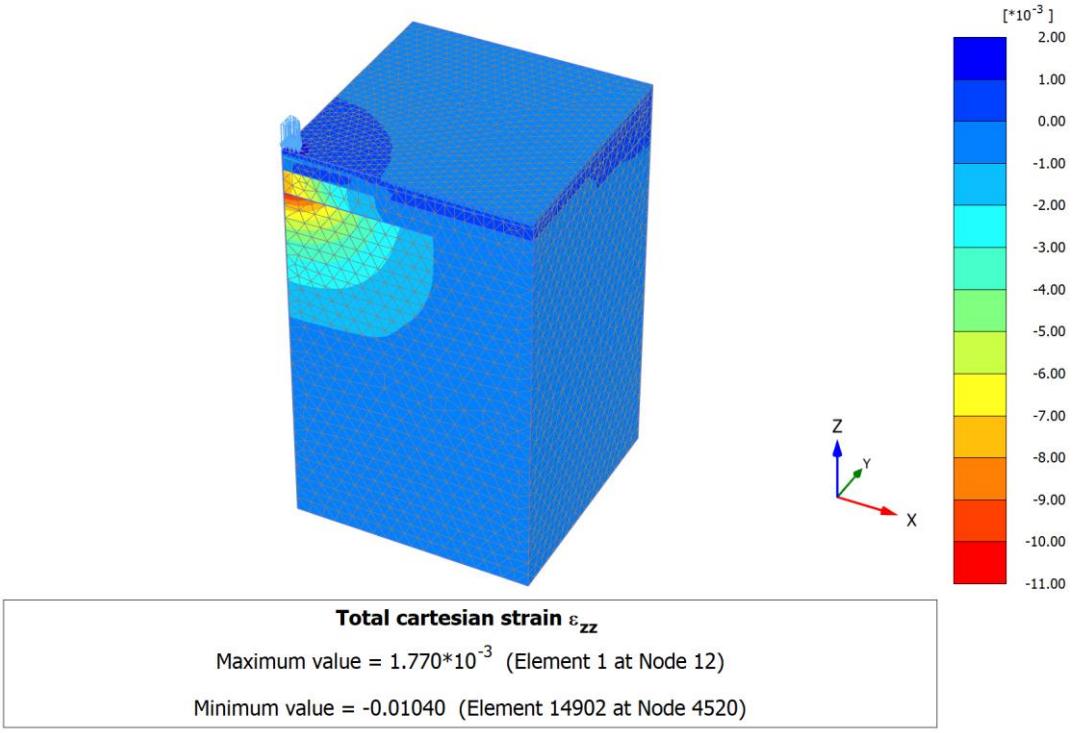

Figure 11. Vertical strains for pavement structure with reinforcement at the bottom of the ESA–sabkha base layer (load 550 kPa)

The analysis results of this research are quantitatively compared with the analysis outcomes of the reported literature. It was seen that in the case of positioning the geogrid between the asphaltic concrete layer and stabilized base, an insignificant reduction in fatigue strains was obtained (2.1%). However, there was a fairly good matching in the reduction (21.1%) noticed in the horizontal strains (fatigue strains) obtained in this research when the geogrid was positioned at the interface of the stabilized base and subbase course layers and the outcomes stated by Dondi, (1994) and *Pandey et al. (2012)* (20 and 22.35%, respectively). These remarkable results may be attributed, as mentioned beforehand, to the stabilization-induced high stiffness of the base course layer. Al-Azzawi (2012) reported the same trend even though the user base course layer was not stabilized. For rutting strains (vertical strains), the maximum reduction occurred when the geogrid was placed at the subgrade layer. This trend was stated and documented in literature by many investigators (*Saad et al. 2006; Wathugala, et al.1996; Moayedi et al. 2009; Kazemian et al. 2010 and Pandey et al. 2012*).

4. COMPARING PLAXIS 3D OUTCOMES WITH LABORATORY TEST RESULTS

To validate the simulation results of Plaxis 3D, simulated pavement layers were constructed in the laboratory and then tested using a Wessex wheel-tracking machine. The geogrid was placed on the sabkha subgrade as the optimum location based on the finite element simulation outcomes discussed beforehand. Two sample models were prepared with lengths of 50 cm and widths of 25 cm. Figure 12 shows the setup of samples on the Wessex wheel tracker. The test is applied under a wheel load of 552 kPa (as used in the Plaxis 3D simulation) by putting sets of weights on each wheel of the tracker (figure 12). Each wheel weighted 18 kg. A static weight of steel plates provides the necessary contact stress (4.5 kg each). In other words, we needed to put eight steel plates (4.5 kg each) on each wheel, so the weight of these plates combined with the wheel's weight, divided by the contact area (1,000 mm^2), gave the required load for testing (552 kPa). The deformation of pavement samples with the number of wheel passes is recorded through the wheel tracker deformation-recording unit. Figure 13 demonstrates the comparison of the vertical deformation resulted from the finite element analysis using the Plaxis 3D software and the laboratory wheel tracking test results. Based on the figure, it is clear that there is a reasonable agreement between the results. This leads to the conclusion that using Plaxis 3D in the FEM can help predict the performance and deformation of the pavement section with stabilized sabkha soil as a base layer properly.

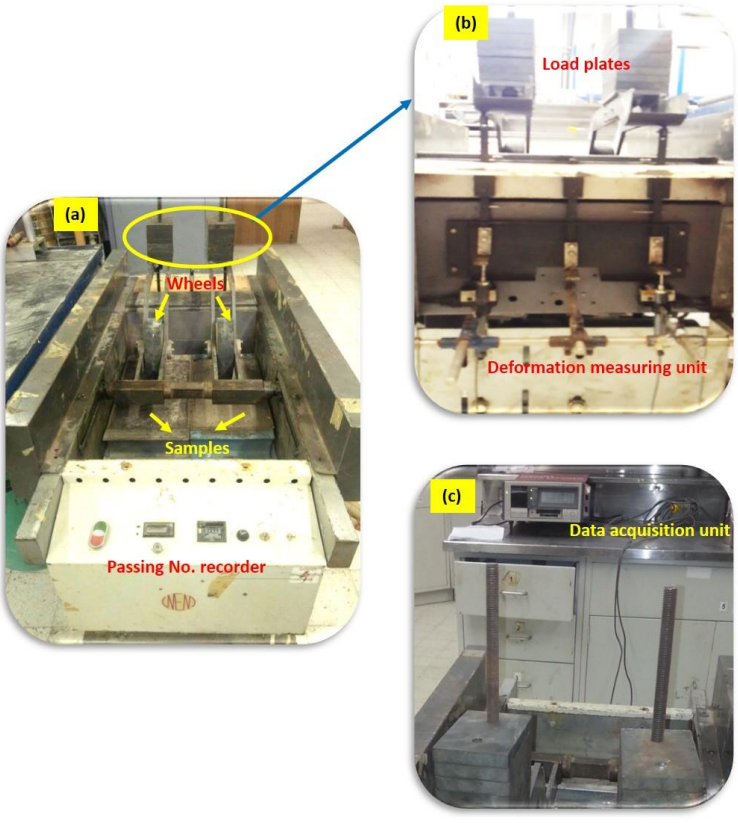

Figure 12. Wheel tracker machine

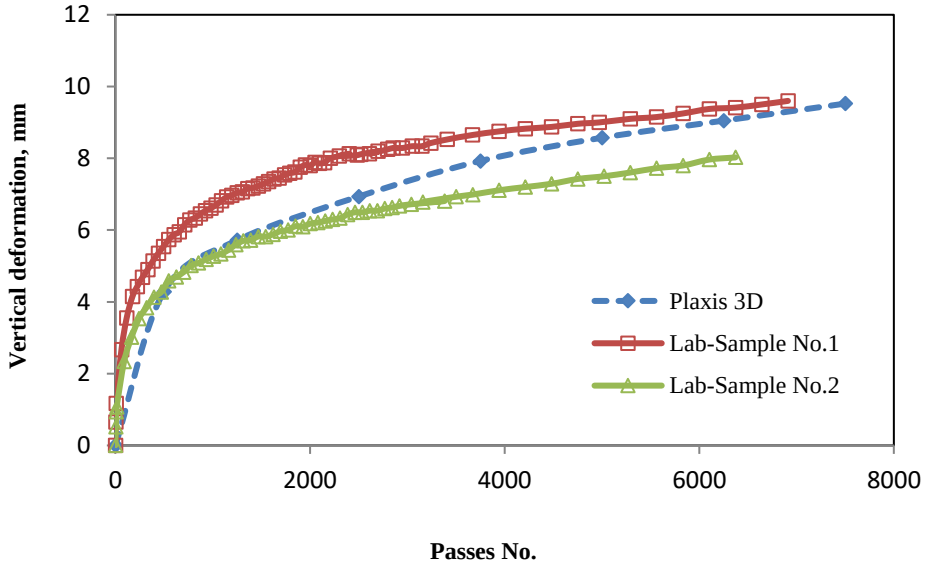

Figure 13. Comparison between the FEM and laboratory test results

5. IMPACT OF GEOGRID REINFORCEMENT ON FATIGUE AND RUTTING LIFE INTERVALS

Based on field examinations and evaluations of pavement surface conditions of most roads, it is found that fatigue cracking and rutting are considered the most significant distresses of pavements structure. The load repetition applied by the moving wheel leads to the initiation of cracking in the asphaltic concrete layer, called fatigue cracking. However, the accumulation of plastic strains in all pavement layers under the repeated loads is called rutting that formed along the wheel path. It is known that horizontal tensile strains (εt^{max}) evolved at the bottom of the asphaltic concrete layer is considered as an index for fatigue distress whereas the vertical compression strains (εc^{max}) is considered as an indicator for the rutting distress. Many models related tensile strains and load repetitions number with fatigue failure and between-load repetitions number and compressive strains for rutting failure (Heukelom and Klomp, 1962; Asphalt Institute, 1982; *Fin et al. 1986*). In this study, the failure criterion for fatigue cracking and rutting was evaluated based on the correlations established by the asphalt institute as follows:

For fatigue,

$$N_f = 0.0796\ (\varepsilon_t)^{-3.291}\ (E)^{-0.854},\ (1)$$

Where

N_f = Load applications number till failure,

ε_t = Horizontal tensile strains at the bottom of the asphaltic layer,

And E = Modulus of elasticity of asphaltic concrete layer.

For permanent deformation (rutting),

$$N_f = 1.365 * 10\ -9\ (\varepsilon_c)^{-4.477},\ (2)$$

Where,

N_f = Load applications number till failure,

And ε_c = Vertical compressive strains at the bottom of the asphaltic layer.

It is well known that damage to pavement structure occurs and develops rapidly under heavier loads. To address the influence of geogrid reinforcement on rutting and fatigue strains, higher axle loads were applied through the 3D finite element model built using the Plaxis 3D software for the unreinforced pavement structure section and geogrid-reinforced pavement structure in which the geogrid membrane was positioned at the sabkha subgrade. The developed horizontal strains, i.e., fatigue strains, at the bottom of the asphaltic concrete layer and vertical compressive strains, i.e., rutting strains, at the top of the sabkha subgrade were used in equations 1 and 2 to deduce the fatigue and rutting life intervals.

The damage (Di) produced by each application of a single axle load can be determined by equation 3:

$$Di = 1/Ni,\ (3)$$

Where Di is known as the accumulative damage and Ni the lowest number of load applications caused either by rutting or fatigue failure, as given by equations 1 and 2. The whole number of load applications (N_f) that are accepted over the pavement service life could be found when the entire accumulative damage (Di) amounts to one. Figure 14 presents the determined fatigue damage ratios against axle loads for unreinforced and geogrid-reinforced pavement structures. A noticeable decrease in fatigue damage was observed in pavements with geogrid reinforcement ranging from 31 to 51% for the various axle loads applied. On the other hand, no significant differences in rutting damage ratio were found, per figure 15, and the reduction in rutting damage ratio ranged from 11 to 25% were noticed for the various applied axle loads. From the results, geogrid is a tensile-resistant material that can mitigate fatigue cracking to a certain degree and its effects in reducing rutting distress is marginal.

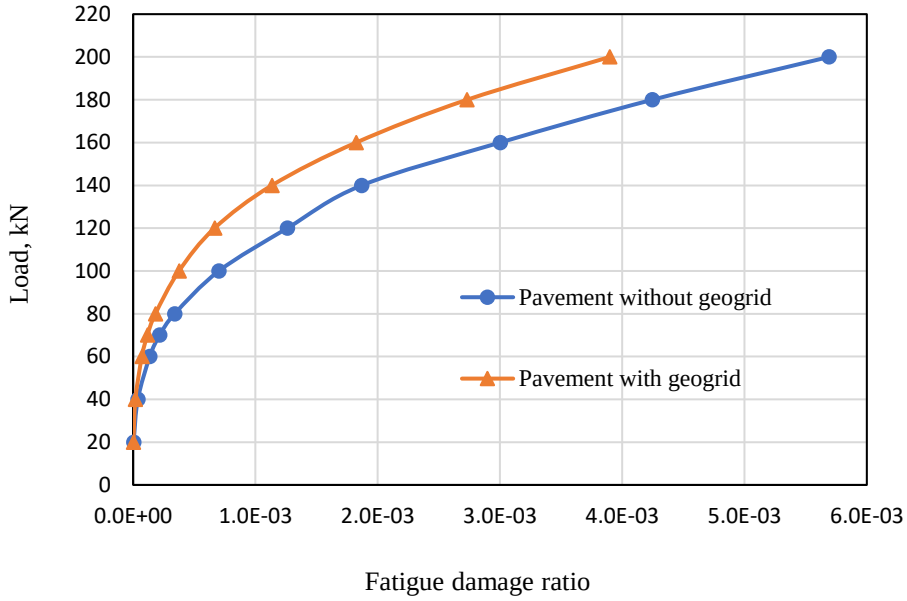

Figure 14. Fatigue damage ratio in unreinforced and reinforced pavement (geogrid is positioned at the sabkha subgrade)

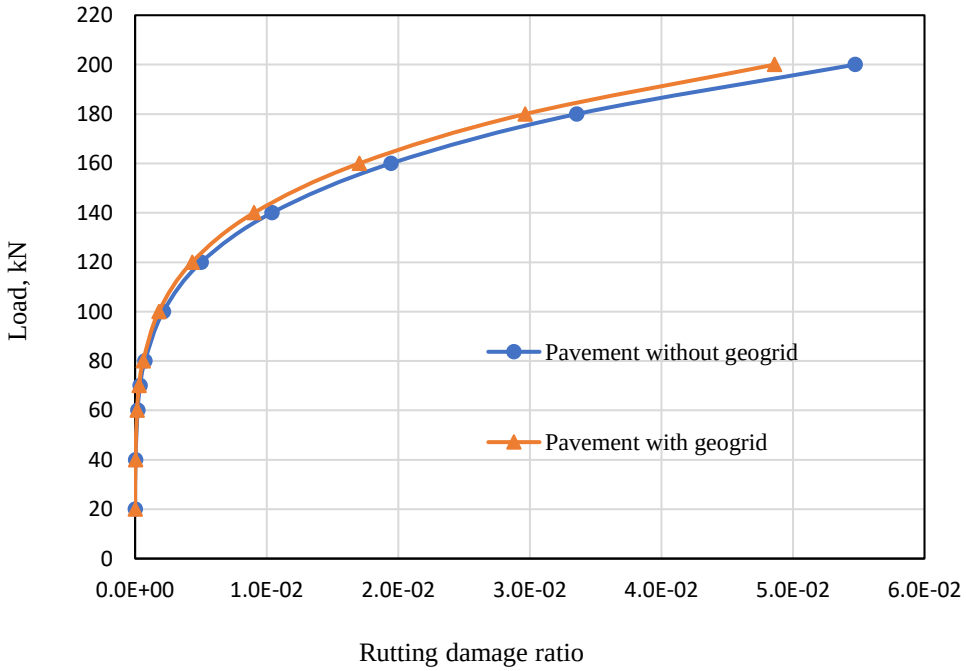

Figure 15. Rutting damage ratio in unreinforced and reinforced pavement (geogrid is positioned at the sabkha subgrade)

6. CONCLUSIONS

A series of 3D finite element simulations were done to estimate the merits of incorporating a layer of geogrid inside the pavement structure having a base layer of marginal sabkha soil stabilized with Emulsified Sulfur Asphalt (ESA). The simulations were done under a parametric investigation to figure out the positive effects of geogrid reinforcement on the rutting and fatigue strains criteria. Based on the outcomes of the simulations, the conclusions are as follows:

When the geogrid was placed at the sabkha subgrade layer, it led to the highest reduction in horizontal tensile strains up to 22.8%. Thus, geogrid reinforcement showed good potential for decreasing fatigue strains in the pavement structure.

No significant differences in the vertical strains were found between reinforced and geogrid-reinforced pavements. The highest reduction was about 5.7%. Similarly, the maximum reduction for vertical displacement was about 3.7%.

Geogrid is a material with tensile stiffness and it can pronouncedly reduce the horizontal strains and, hence, fatigue cracking. However, its effect in reducing vertical displacement is marginal.

Geogrid reinforcement decreased the fatigue damage ratio significantly (31 to 51%) while the reduction in rutting damage ratio was a little bit lower (11 to 25%).

Positioning geogrid on the subgrade leads to a higher reduction in fatigue and rutting strains and vertical displacement.

Geogrid reinforcement enhanced the performance of the pavement structures consisting of stabilized sabkha with emulsified sulfur asphalt base layer, which was resting at the marginal sabkha subgrade and was usable for low-to-moderate traffic volume.

The results of the finite element program Plaxis 3D were in good agreement with the results of the laboratory experimental tests.

Finite element modeling using geotechnical-based software (i.e Plaxis 3D) is a powerful and reliable tool to predict the performance of pavement structure material under traffic loading.

FUNDING

This research did not receive any specific grant from funding agencies in the public, commercial, or nonprofit sectors.

CONFLICT OF INTERESTS

The author declares that he has no conflicts of interest to report regarding the present study.

REFERENCES

1. Abdhesh K. S., Satish C., Praveen, K. (2014). Finite element analysis of flexible pavement with different subbase materials, Indian Highway 42(2014) pp.57-67.
2. Abdullah G.M.S., Al-Abdul Wahhab H.I. (2015). Evaluation of foamed sulfur asphalt stabilized soils for road applications. Constr Build Mater 2015;88:149–58, http://dx.doi.org/10.1016/j.conbuildmat.2015.04.013
3. Abdullah G.M.S., Al-Abdul Wahhab H.I. (2018). Stabilisation of soils with emulsified sulphur asphalt for road applications. Road Mater Pavement Des 2018, http://dx.doi.org/10.1080/14680629.2018.1436465
4. Abduljauwad S.N, Al-Amoudi O.S. (1995). Geotechnical behavior of saline sabkha soils. Geotechnique 45(3):425–445, https://doi.org/10.1680/geot.1995.45.3.425
5. Akili, W. (2006). Salt encrusted desert flats (sabkha): problems, challenges and potential solutions. In: Proceedings of the fourth international conference on unsaturated soils, Carefree, AZ, The Geo-Institute of the ASCE, Reston, VA, pp 391–402, http://dx.doi.org/10.1061/40802(189)28
6. Alex, A. (2000). Characterization of unbound granular layers in flexible pavements. Report No. ICAR /502-3, Texas Transportation Institute.

7. Al-Homidy A.A, Dahim M. H., Abd El Aal, A.K. (2017). Improvement of geotechnical properties of sabkha soil utilizing cement kiln dust. Journal of Rock Mechanics and Geotechnical Engineering Volume 9, Issue 4,Pages 749-760, http://dx.doi.org/10.1016/j.jrmge.2016.11.012
8. Al-Mehthel, M., Al-AbdulWahhab, H. I., Hussein, I. A., & Al-Idi, S. H. (2017). Foamed sulfur asphalts for pavement recycling and soil stabilization. *Patent Number: 11201604034Y* (Docket Number: SA5095-06).
9. Al-Azzawi A. A. (2012). Finite element analysis of flexible pavements strengthened with geogrid. ARPN J Eng Appl Sci 7(10):1295–1299.
10. Asphalt Institute (1982). Research and development of Asphalt Institute's Thickness Design Manual. 9th Ed., Research Report 82-2, The Asphalt Institute.
11. Berg, R. R., Christopher, B. R., and Perkins, S. W. (2000). Geosynthetic reinforcement of the aggregate base course of flexible pavement structures. GMA White paper II, Geosynthetic material Association, Roseville, MN, USA, 130p.
12. Bolton, M. D. (1986). The strength and dilatancy of sands. Geotechnique, 36, No. 1, 65–78, http://dx.doi.org/10.1680/geot.1986.36.1.65
13. Dondi, G. (1994).Three-dimensional finite element analysis of a reinforced paved road, 5th Int.Conf. on Geotextiles, Geomembranes and Related Products, Vol. 1, Singapore, pp.95–100.
14. Finn, F., Saraf, C. L., Kulkarni, R., Nair, K., Smith, W., and Abdullah, A. (1986). ''Development of pavement structural subsystems.''*NCHRP Rep. 291*, Transportation Research Board, Washington, D.C.
15. Heukelom W, Klomp AJG (1962). Dynamic testing as a means of controlling pavements during and after construction. Proceedings of the Int. Conference on the Structural Design of Asphalt Pavement, Ann Arbor, Michigan, U.S.A.
16. Howard, I.L. and Warren, K.A. (2009), Finite-element modelling of instrumented flexible pavements under stationary transient loading, J. Transportation Eng. ASCE, 135(2): 53-61, https://doi.org/10.1061/(ASCE)0733-947X(2009)135:2(53)
17. Ibrahim, E.M., El-Badawy, S.M., Ibrahim, M.H., Gabr, A., and Azam, A. (2017) "Effect of geogrid reinforcement on flexible pavements." Innovative Infrastructure Solutions, 2(54), pp. 1-15, http://dx.doi.org/10.1007/s41062-017-0102-7
18. Kazemian, S., Barghchi, M., Prasad, A., Maydi, H. and Huat, B.K. (2010). Reinforced pavement above trench under urban traffic load: Case study and finite element (FE) analysis, Journal of Scientific Research and Essay Vol. 5 (21), Nov.4, 2010, pp. 3313- 3328.
19. Ling, H. Liu, H. (2003). Finite element studies of asphalt concrete pavement reinforced with geogrid. Journal of Engineering Mechanics, ASCE, 129(2003), pp.801–811, http://dx.doi.org/10.1061/(ASCE)0733-9399(2003)129:7(801)
20. Majedi, P., Ghalehjough, B., Akbulut, S., and Çelik, S. (2017). Effect of reinforcement on stability and settlement of embankment: A finite element analysis of different kinds of reinforcing and construction conditions. European Journal of Advances in Engineering and Technology, 2017, 4(10): 759-764.
21. Mirmoradi, S. H. and Ehrlich, M. (2015a). Modeling of the compaction-induced stress on reinforced soil walls. Geotextiles and Geomembranes, 43, No. 1, 82–88, http://dx.doi.org/10.1016/j.geotexmem.2014.11.001
22. Moayedi, H., Kazemian, S., Prasad, B. and Huat (2009). Effect of geogrid reinforcement location in paved road improvement, Journal of EJGE, Vol.14, pp.3313-3329.
23. Mousavi, S.H., Gabr, M. & Borden, R., (2017). Optimum location of the geogrid reinforcement in unpaved road. Canadian Geotechnical Journal, Vol. 54. , pp 1047 – 1054, http://dx.doi.org/10.1139/cgj-2016-0562
24. Pandey, S., Ramachandra Rao, K., and Tiwari D. (2012). Effect of geogrid reinforcement on critical responses of bituminous pavements. 25th ARRB Conference – Shaping the future: Linking policy, research and outcomes, Perth, Australia 2012.
25. Perkins, S. W. (2001). Mechanistic-empirical modeling and design model development of geosynthetic reinforced flexible pavements. Montana Department of transportation, Helena, Montana, Report No. FHWA/MT-01-002/99160-1A.
26. Perkins, S. W. (2002). Evaluation of geosynthetic reinforced flexible pavement systems using two pavement test facilities. Report No. FHWA/MT-02-008/20040, U.S. Department of Transportation, Federal Highway Administration.

27. Saad, B., Mitri, H. and Poorooshasb, H.J. (2006), 3D FE analysis of flexible pavement with geosynthetic reinforcement, Journal of Transportation Engineering, Vol.132, No.5, ASCE, pp.402-415, http://dx.doi.org/10.1061/(ASCE)0733-947X(2006)132:5(402)
28. Schanz, T., Vermeer, P. A. and Bonnier, P. G. (1999). The hardening soil model: formulation and verification. Proceedings of Beyond 2000 in Computational Geotechnics, Rotterdam, Netherlands, pp. 281–296, http://dx.doi.org/10.1201/9781315138206-27
29. Sukumaran, B. Chamala, N. Kyatham, V.(2004).Three-dimensional finite element modeling of flexible pavements, FAA worldwide airport technology transfer conference, Atlantic city, New Jersey, USA, (2004) pp.1-12, http://dx.doi.org/10.1061/40776(155)7
30. Tapase, A., and Ranadive, M. (2016). Performance evaluation of flexible pavement using finite element method. In: ASCE GSP 266, Geo-China 2016: Material, Design, Construction, Maintenance and Testing of Pavement, pp. 9–17, http://dx.doi.org/10.1061/9780784480090.002
31. Wathugala, G. W., B. Huang and S. Pal. (1996). Numerical simulation of geosynthetic-reinforced flexible pavements. Transportation Research Record 1534, Transportation Research Board, National Research Council, Washington, D.C., USA. pp. 58-65, https://doi.org/10.1177/0361198196153400109